# Dimerization enhancement in one-dimensional Hubbard and Pariser-Parr-Pople models

G. W. Hayden and Z. G. Soos
*Department of Chemistry, Princeton University, Princeton, New Jersey 08544*
(Received 16 March 1988)

The Su-Schrieffer-Heeger model for polyacetylene (PA) is generalized to electron-electron (*e-e*) contributions in Hubbard and Pariser-Parr-Pople (PPP) models. The equilibrium dimerization $\delta$ is found via the Hellmann-Feynman theorem. Exact results, computed by a valence-bond method, are presented for $N \leq 14$ site systems. $N=4n+2$ rings are lower bounds on the dimerization, due to a finite-size gap at $\delta=0$, while $N=2n$ chains give upper bounds, thereby facilitating $N\rightarrow\infty$ extrapolations. Enhanced dimerization is demonstrated in the PA regime of $\delta\sim 0.05$–$0.10$, although the enhancement is less than previous estimates. Dimerization is suppressed for $\delta > 0.40$ in Hubbard models, as understood in terms of competing effects involving the band gap and bandwidth. Additional enhancement is found in PPP models due to the distance dependence of the potential $V(R)$, primarily through the gradient $V'(R_0)$ at the spacing of the regular array. Molecular PPP parameters are then consistent with the PA ground state, including the dimerization, optical gap, and backbone vibrational frequencies.

## I. INTRODUCTION

Much recent attention has been given to electron-electron (*e-e*) contributions to the ground-state dimerization of polyacetylene (PA), to modeling the PA $\pi$-band, and to the relation of PA to other conjugated molecules and polymers.[1,2] Several independent approaches[3–8] have established that *e-e* correlations initially increase the dimerization of Hubbard models. The behavior of the infinite system is inferred from extrapolations of exact finite-size results[3–5] and by perturbation[7] or variational methods.[6] We extend exact results to an $N=14$-site system using a previously described[9] valence-bond method, construct upper and lower bounds to the infinite system, and provide an intuitive picture to explain trends in the tendency to dimerize. Our results for the infinite system are essentially quantitative for large dimerization and semiquantitative for the PA dimerization, for any *e-e* interaction in Hubbard or in Pariser-Parr-Pople (PPP) models. The distance dependence of the *e-e* potential $V(R)$ leads to additional enhancement of the dimerization through a $V'(R_0)$ contribution, where $R_0$ is the mean C—C bond length. The wide applicability of PPP models[10,11] to conjugated molecules is thereby extended to the PA dimerization[12] without changing microscopic parameters.

A generic PA ground-state energy per site, $\varepsilon_T(u)$, is sketched in Fig. 1 for alternating bond lengths $R_0\pm u$. The Su-Schrieffer-Heeger[13] (SSH) result for $\varepsilon_T(u)$ serves as a reference. The SSH model has noninteracting $\pi$ electrons, linear electron-phonon (*e*-ph) coupling $\alpha$, and a harmonic lattice with force constant $K$. Within the Born-Oppenheimer approximation, the Peierls instability of the half-filled band leads in Fig. 1 to dimerization $\pm u_0$. The ground state is doubly degenerate, since partial double and single bonds can be interchanged in the infinite polymer. Thus $u_0$ and $\varepsilon_T(u)$ are completely specified by $\alpha$, $K$, and the bandwidth $4|t|$. The logarithmic divergence of $\varepsilon_T''(0)$ results in the Peierls instability for noninteracting electrons. Exact results[14] for $\varepsilon_T(u)$ near $u=0$ are also known for linear Heisenberg chains, the strong coupling limit of half-filled Hubbard or PPP models. It is more difficult in general to compute $\varepsilon_T(u)$ near $u=0$. Fortunately, the observed behavior of PA reflects the equilibrium dimerization $u_0$ in Fig. 1.

The general $\pi$-electron problem for a harmonic lattice leads in the Born-Oppenheimer approximation to

$$\varepsilon_T(u)=\varepsilon(u)+\tfrac{1}{2}Ku^2 . \tag{1}$$

The $\pi$-electron ground-state energy per site, $\varepsilon(u)$, is of central interest. All $\sigma$-electron effects are lumped in $K$. All recent studies invoke (1) and linear *e*-ph coupling $\alpha$, but differ in the choice of the $\pi$-electron Hamiltonian, $H$, in the values of the microscopic parameters, and in the approximations or extrapolations for $\varepsilon(u)$. The equilibrium dimerization in Fig. 1 follows from the Hellmann-

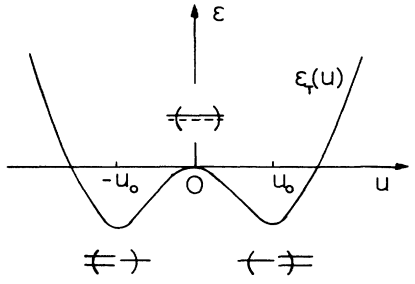


FIG. 1. Schematic representation of the PA ground-state energy per site, $\varepsilon_T(u)$, for alternating partial single and double bonds $R_0\pm u$.

 

Feynman theorem,

$$Ku_0 = -\varepsilon'(u_0) = -\langle \psi | (\partial H/\partial u)_0 | \psi \rangle / N \ , \tag{2}$$

where $\psi$ is the exact ground state of $H$. We may consider (2) to *define* the force constant $K$ needed to maintain equilibrium at dimerization $u_0$. The SSH model then fixes a value for $K_0(u_0)$ and any $e$-$e$ potential $V(R)$ leading to a larger $K(u_0)$ enhances the dimerization. Thus (2) allows comparisons for arbitrary $K$ in (1).

The simplest on-site $e$-$e$ contributions $U = V(0)$ are retained in Hubbard models. Exact solutions[15] for $\varepsilon(0, U)$ are known for regular bond lengths. Most discussions of $e$-$e$ effects on dimerization have been in terms of Hubbard models, as discussed by Dixit and Mazumdar[3] and by Baeriswyl and Maki.[6] The dimerization $u_0$ increases strongly up to $U \sim 4 | t |$ and decreases for larger $U$ in variational or finite-size calculations. We extend in Sec. II exact Hubbard analysis to $N = 14$ sites using a valence-bond technique and obtain both upper and lower bounds on $-\varepsilon'(u)/u$ for the infinite system. Finite $N = 14$ rings converge to the infinite chain for $\delta > 0.3$, while the physical regime, with bond alternation of $\delta = \alpha u_0/t \sim 0.07$, is semiquantitative. We find that some previous results overestimate the maximum dimerization enhancement. We also discuss competing effects on the dimerization which lead to the observed trends in the data.

The Hubbard model has limited applicability to PA and at least a nearest-neighbor $e$-$e$ term $V(R_0 \pm u_0)$ is needed. The Coulomb potential has been used in molecules and is incorporated into the PPP model for conjugated systems, where $V(R)$ is interpolated between $U$ at $R = 0$ and $e^2/R$ at large $R$. As shown in Sec. III, the distance dependence leads to a $V'(R_0)$ contribution in (2) that enhances dimerization in a way not possible for Hubbard models. Both $e$-$e$ and $V'(R_0)$ contributions are instrumental in reconciling[12] molecular values for $t$, $\alpha$, and $K$ with the observed PA dimerization, optical gap, and C-C stretching frequencies.

The PPP model then approximates the $\pi$-electronic states of both conjugated molecules and polymers.[1] Many potential improvements, all requiring greater computational effort, can be cited: $\sigma$-$\pi$ separability in (1) is certainly approximate, as is the choice of a harmonic lattice with a single degree of freedom, linear $e$-ph coupling, and a Born-Oppenheimer description. Even within $\pi$-electron theory, the zero-differential overlap (ZDO) approximation of the PPP model has been extensively discussed.[10,16,17] Like the Hubbard model in other contexts, the PPP model represents a useful compromise between physical realism and computational ease. With these ideas in mind, we consider the equilibrium dimerization of finite Hubbard and PPP chains and rings.

## II. DIMERIZATION IN HALF-FILLED HUBBARD MODELS

We consider $N$ electrons in $N$ orbitals $\phi_n$ and on-site $e$-$e$ interactions $U$ in the Hubbard model:

$$H = -|t| \sum_{n\sigma} [1 - (-1)^n \delta](a^\dagger_{n\sigma} a_{n+1\sigma} + a^\dagger_{n+1\sigma} a_{n\sigma}) + U \sum_n a^\dagger_{n\alpha} a^\dagger_{n\beta} a_{n\beta} a_{n\alpha} \ . \tag{3}$$

The transfer integrals $t(1 \pm \delta)$ alternate in the electronic ground state. We take $t = t(R_0) \sim -2.4$ eV and retain the linear term in $u = R - R_0$ for the $e$-ph coupling constant $\alpha$,

$$t(R_0 + u) = t(1 + \alpha u/t) \ . \tag{4}$$

Dimerization $u$ in (1) then requires alternation $\delta = \alpha u/t$ in (3). The half-filled ground state $\psi$ has by far the simplest geometry. The SSH model corresponds to $U = 0$ in (3) and its solution was originally discussed by Longuet-Higgins and Salem.[18]

The $U$ term in (3) is independent of the dimerization. The equilibrium result (2) consequently involves only the kinetic energy and $\langle \partial H/\partial \delta \rangle$ reduces to Coulson's mobile $\pi$-bond order,[19]

$$p(\delta, U) = \frac{1}{2} \left\langle \psi \left| \sum_\sigma (a^\dagger_{n\sigma} a_{n+1\sigma} + a^\dagger_{n+1\sigma} a_{n\sigma}) \right| \psi \right\rangle \ . \tag{5}$$

We take $\delta > 0$ and $\delta < 0$, respectively, for partial double bonds $t(1+\delta)$ and single bonds $t(1-\delta)$ in the exact ground state $\psi(\delta, U)$. We change variables to $\delta = \alpha u/t$ and rearrange (2), to obtain the dimensionless ratio

$$|t| K/\alpha^2 = [p(\delta, U) - p(-\delta, U)]/\delta \equiv \Delta p(\delta, U)/\delta \tag{6}$$

which is $2/\pi\lambda$ in solid-state approaches[6] for the dimensionless $e$-ph parameter $\lambda$. Dimerization effects in Hubbard models reflect kinetic energy, or bond order, changes through $\psi(\delta, U)$. The exact result (6) is not immediately applicable, however, since $p(\delta, U)$ for $U \neq 0$ is known only at $\delta = 0$ and 1.

The Hückel ($U = 0$) result in (6) is[18]

$$\frac{\Delta p(\delta, 0)}{\delta} = \frac{4\{K[(1-\delta^2)^{1/2}] - E[(1-\delta^2)^{1/2}]\}}{\pi(1-\delta^2)} \ , \tag{7}$$

where $K$ and $E$ are complete elliptic integrals of the first and second kind, respectively. The logarithmic divergence of (7) as $\delta \to 0$ is the Peierls instability. For $\delta > 0$, $\Delta p(\delta, 0)/\delta$ defines the reference force constant $K_0(u_0 = t\delta/\alpha)$ in (2) for dimerization $u$ in the SSH model. The dimerization problem for Hubbard models thus reduces to the $U$ dependence of $\Delta p(\delta, U)$.

We begin with exact results for finite Hückel models, where the $N \to \infty$ limit is known to be (7). Alternating Hückel rings lead to the $|t| K/\alpha^2$ curves in Fig. 2 and illustrate the problems encountered in finite systems. The $N = 4n$ and $4n + 2$ rings form separate series that converge to (7) from above and below, respectively, forming a funnel, and neither series has the proper $\delta$ dependence. The $\delta = 1$ limit of decoupled dimers is independent of $N$ for even rings. In Fig. 2 convergence is indeed more rapid at large $\delta$. Dimerization opens a gap of order $\delta$. The ground-state energy of rings with $N > \delta^{-1}$ converges very rapidly, as can be verified in alternating Hückel or Heisenberg rings in which large $N$ is accessible.[20] The

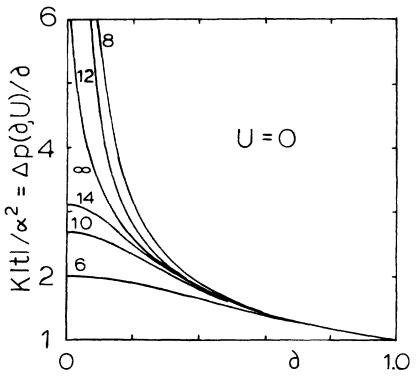


FIG. 2. Force constant $K$ for equilibrium dimerization $\delta=\alpha u/t$ in Hückel rings. The $4n$ and $4n+2$ rings converge to the infinite system, Eq. (7), from above and below, respectively.

implication is that $N=14$ is essentially quantitative for $\delta>0.3$.

The $\delta=0$ behavior reflects the nondegenerate ground state and finite gap of order $N^{-1}$ in $4n+2$ rings, which consequently require smaller $K$ to maintain some dimerization than the infinite chain. The electronic degeneracy and Jahn-Teller instability of $4n$ Hückel rings, on the contrary, requires a stiffer lattice than in the infinite case. The ground-state energy per site $\varepsilon(0,0,N)$ of regular Hückel rings is

$$\varepsilon(0,0,N)/4\,|\,t\,|=N^{-1}\cot(\pi/N)\sim-\pi^{-1}+\pi/3N^2$$
$$=-N^{-1}\csc(\pi/N)\sim-\pi^{-1}-\pi/6N^2 \quad (8)$$

for $N=4n$ and $4n+2$, respectively. Since $\varepsilon(1,0)=-2\,|\,t\,|$ is independent of $N$, the convergence of $4n$ rings from above in (8) implies that $-\varepsilon'(\delta,0,N)/\delta$ also converges from above. Conversely, $4n+2$ rings converge from below. We similarly expect even chains to converge from above. Removal of the bond between sites 1 and $N=2n$ leads to a higher energy than in rings. At $\delta=0$, the energy per site converges from above with increasing $N$, while $\delta\to1$ again reduces to $N/2$ decoupled dimers whose energy $\varepsilon(1,0)$ is independent of $N$.

The $4n+2$ series in Fig. 2 thus provides lower bounds for $\Delta p(\delta,0)/\delta$. The result holds for arbitrary $U>0$ in (3). Hashimoto[21] has solved the Lieb-Wu equations up to $N=4n+2=50$ and finds $\varepsilon(0,U,N)$ to converge from below to the known value of $\varepsilon(0,U)$. The dimer limit $\delta=1$ is again trivial and independent of $N$. Thus $-\varepsilon'(0,U,N)/\delta=\Delta p(0,U,N)/\delta$ converges from below. The large $U$ limit of (3) leads to Heisenberg antiferromagnetic chains with $J=2t^2/U$ at $\delta=0$. Regular even rings again converge from below to Hulthén's exact result[22] and alternating even rings converge from below for arbitrary $\delta$ for the numerically accessible $N\lesssim26$ systems.[20] Direct solutions of $N=4n+2\lesssim14$ Hubbard and PPP rings with arbitrary $\delta$ also show $|\,t\,|K/\alpha^2$ to converge from below. The finite-size gap at $\delta=U=0$ makes $4n+2$ rings less susceptible to dimerization even when $e$-$e$ interactions are strong.

The $4n$ series are not upper bounds, however, for $U>0$. Finite $U$ opens a gap at $\delta=0$, suppressing the Jahn-Teller instability, and produces a nondegenerate singlet ground state. In the Heisenberg (large $U$) limit, the energy per site of the $4n$ series merges with the $4n+2$ series and converges from below. The crossover with $\varepsilon(0,U)$ occurs at larger $N$ for smaller $U$ and reflects competition between finite-size energy splittings and the correlation gap. These expectations are confirmed by Fig. 3. The $U=2\,|\,t\,|$ curves of $\Delta p(\delta,U,N)/\delta$ in Fig. 3(a) have no crossings between $4n$ and $4n+2\lesssim14$. The correlation gap is so small that $4n$ rings are still more susceptibile to dimerization. But the $U=4\,|\,t\,|$ and $8\,|\,t\,|$ curves in Figs. 3(b) and 3(c) show crossovers at $N<14$, as expected from the behavior of Heisenberg rings.

The rapid convergence with $N$ persists in Fig. 3 for $U>0$. Indeed, the variations from the infinite curve in Fig. 2 are suppressed with increasing $U$, which tends to localize charges and opens a correlation gap in any half-filled system. The PA values of $1<U/|\,t\,|<2$ and $\delta=0.07$ are closest to Fig. 3(a), where reasonable estimates can be made down to $\delta\sim0.1$. The $U=4\,|\,t\,|$ funnel in Fig. 3(b) disappears below $\delta\sim0.20$ and another extrapolation method is then needed. The Peierls instability at $\delta\to0$ cannot be extracted from such small systems.

It is advantageous to replot the $\Delta p(\delta,U)/\delta$ curves as a function of $U/|\,t\,|$ for fixed $\delta$, as shown in Fig. 4 for $\delta=0.05$, 0.10, 0.20, and 0.40. The $N\to\infty, U=0$ result (7) is marked on each panel. Any dimerization enhancement can readily be compared for either the finite or infinite Hückel ring. The lower bounds provided by the $4n+2$ series, in particular, clearly demonstrate enhanced dimerization at $\delta=0.05$ or 0.10, where $N=14$ curves with $U/|\,t\,|>0$ are above the $N\to\infty$ Hückel point. $N=14$ rings involve some $11\times10^6$ Slater determinants with $S_z=0$ or almost $2.8\times10^6$ VB diagrams with $S=0$; spatial and electron-hole symmetry leads to sparse matrices of $10^5\times10^5$ that are about 100 times larger than the $N=10$ rings solved by Dixit and Mazumdar.[3] The $\delta=0.20$ panel shows that the infinite curve can be es-

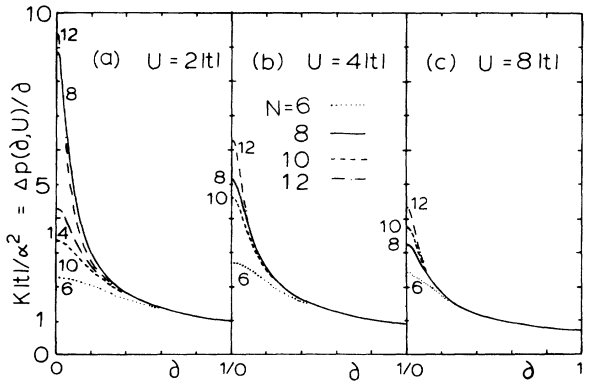


FIG. 3. Force constant $K$ for equilibrium dimerization $\delta=\alpha u/t$ in finite Hubbard rings at (a) $U=2\,|\,t\,|$, (b) $U=4\,|\,t\,|$, and (c) $U=8\,|\,t\,|$.

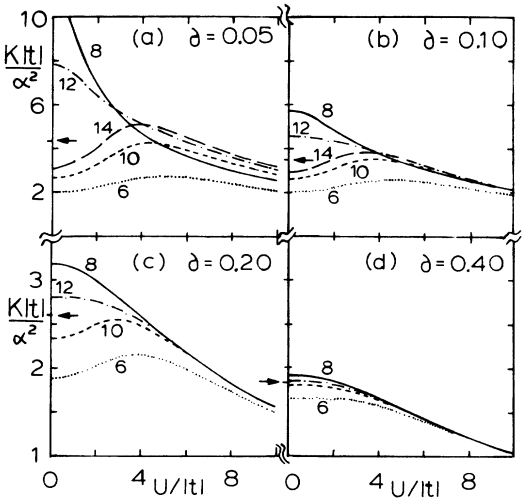


FIG. 4. Force constant $K$ vs $U/|t|$ for equilibrium dimerization (a) $\delta=0.05$, (b) $\delta=0.10$, (c) $\delta=0.20$, and (d) $\delta=0.40$ in finite Hubbard rings. The arrow marks the $N\rightarrow\infty, U=0$ value.

timated fairly well for any $U/|t|$. Convergence is even better at larger $\delta$. There is hardly any enhancement at $\delta=0.20$ and dimerization is suppressed for $\delta\gtrsim 0.4$.

Even chains with $N/2$ double bonds $t(1+\delta)$ and $N/2-1$ single bonds $t(1-\delta)$ in (3) always have higher energy than that of the corresponding ring, which has an extra single bond between sites 1 and $N$. The boundary condition becomes irrelevant as $N\rightarrow\infty$. As mentioned above, $\varepsilon'$ for even chains also converges to the infinite chain result from above, implying that the $\Delta p(\delta,U)/\delta$ curves for finite chains provide upper bounds to $|t|K/\alpha^2$ in (6). The infinite curve is consequently bracketed by even chains and $4n+2$ rings. The physically important regime of $\delta=0.05$ and $\delta=0.10$ is shown in Fig. 5.

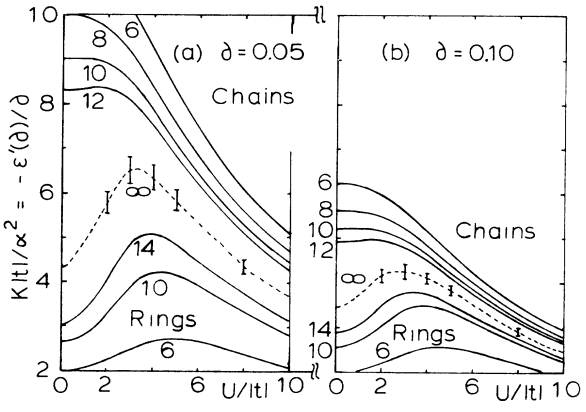


FIG. 5. Force constant $K$ vs $U/|t|$ for Hubbard rings with $N=4n+2$ and chains with $N=2n$ for equilibrium dimerization (a) $\delta=0.05$ and (b) $\delta=0.10$. Rings and chains provide upper and lower bounds for the infinite system (dashed line) based on results at $U/|t|=2$, 3, 4, 5, and 8. The error bars reflect different extrapolations.

Using Figs. 3–5 we could obtain a fairly good estimate of the position of the infinite curves. To improve the estimate we have carried out extrapolations of the chain and ring results as a function of $1/N$, as in Fig. 6. The missing bond in chains largely cancels in $\varepsilon'(\delta)$ and results in comparable convergence for chains and rings, albeit from opposite sides. The curves intersect in a region of finite $N$ for which the values have essentially converged to the infinite result. We have indicated our best estimates for the infinite curves in Fig. 5 based on $1/N$ and $1/N^2$ extrapolations, and the averages of chain and ring curves. For larger $\delta$, the error bars would be quite small, while for smaller $\delta$, estimation of the infinite curve is difficult given data for $N\leq 14$.

We would now like to understand some of the effects on the dimerization that lead to enhancement and subsequent reduction, as well as to shifts in the peaks seen in our data and in previous work.[3,6] As $U$ goes from the Hückel ($U=0$) to Heisenberg ($U\rightarrow\infty$) limits in (3), there is a competition between the increasing Peierls instability, as given by $\varepsilon_T'(\delta)$ for $\delta\rightarrow 0$, and decreasing electronic energy scale. At $U=0$, the kinetic energy is of order $t$ per electron, while at large $U$ we have localized spins with energy $J\sim t^2/U$ per electron. Increasing $U$ thus decreases the available electronic energy in (1) and, as already noted, decreases the dimerization for fixed $t$, $\alpha$, and $K$. On the other hand, near $\delta=0$, the Hückel energy goes as $t\delta^2\ln\delta$, while the Heisenberg result[14] has a stronger divergence of $J\delta^{4/3}\ln\delta$. Bosonization[23] of the Heisenberg antiferromagnet leads to $\delta^{4/3}$ behavior, without the logarithmic factor, and already produces a stronger divergence than in Hückel theory. The exponent in Hubbard models presumably goes from $\delta^2$ at $U=0$ to $\delta^{4/3}$ as $U\rightarrow\infty$. Although the instability is greater in the Heisenberg limit, the reduced ($J\sim t^2/U$) electronic energy leads to small dimerization. Spin-Peierls systems are rare[24] because a typical $J\sim 0.01$ eV requires an extremely soft mode. The distinction between correlation contributions to the Peierls instability and to the equilibrium dimerization has not previously been emphasized.

We can further examine the competing effects of $U$ on dimerization by looking at the bond orders $p(\delta,U)$ defined by (5). For $U=0$ the bond orders[18] are shown in Fig. 7. They range from $p(0,0)=2/\pi$ to $p(1,0)=1$ and $p(-1,0)=0$. The bond-order difference $\Delta p(\delta,U)$ in (6) fixes any change in the dimerization. Although $p(\delta,U)$ is

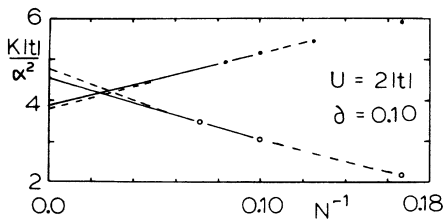


FIG. 6. Force constant $K$ vs $N^{-1}$ at $U=2|t|$ and $\delta=0.10$ for chains (●, top) and rings (○, bottom). The solid (dashed) lines are linear (quadratic) extrapolation for the last 2 (3) points.

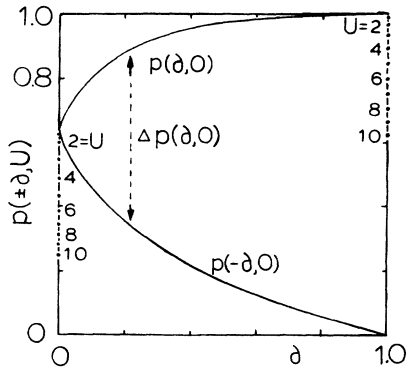


FIG. 7. Alternation dependence of the bond orders $p(\pm\delta, U)$ in Eq. (5). The $U=0$ results are given by the solid line; the $\delta=0,1$ values are exact for infinite Hubbard rings; $\Delta p(\delta, U)/\delta$ in Eq. (7) gives the tendency for dimerization.

not known exactly in general, the exact $\delta=0$ and $\delta=1$ values for $U=n\,|\,t\,|$ in Fig. 7 are readily found. Quite generally, we have $p(-1, U)=0$ for any $U$ and

$$p(1, U)=[1+(U/8t)^2]^{-1/2}\ . \tag{9}$$

At large $\delta$, $p(-\delta, U)$ is almost zero, so that the decrease in $p(\delta, U)$ leads to a decrease in $\Delta p(\delta, U)$ and to reduced alternation, as shown for $\delta=0.4$ in Fig. 4(c). At $\delta=0$, where the Peierls instability is most important, the initial decrease of $p(0, U)$ in Fig. 6 is faster than that of $p(1, U)$. It is plausible that most of the difference in the rate of change with $U$ is taken up near $\delta=0$, and since $U/t(1+\delta)$ for the double bonds is less than $U/t(1-\delta)$ for the single bonds, $p(\delta, U)$ decreases less than $p(-\delta, U)$. This leads to an initial increase in $\Delta p(\delta, U)$, rationalizing the enhancement at small $\delta$ and $U<4\,|\,t\,|$.

Increasing $\delta$ at small $U/|\,t\,|$ then leads to less of an increase in kinetic energy due to $U$, with the difference showing up primarily on the double bonds. The enhancement of the double bonds is associated with an increased antiferromagnetic nearest-neighbor spin correlation $4\langle \mathbf{S}_{zn}\cdot\mathbf{S}_{zn+1}\rangle$ across the double bonds, as shown in Fig. 4 of Ref. 5. This type of coupling favors hopping due to the exclusion principle and is known to increase[25] with $U$, from $-2/\pi^2$ at $U=\delta=0$ to $-(4\ln 2-1)/3$ at large $U$. At smaller $U$, we believe that the increased spin coupling occurs because whenever two electrons occupy the same site, $U$ more quickly causes one of the spin-paired electrons to leave the site. The electron preferentially hops across the double bond. This effect is the likely source of the increasing Peierls instability at $\delta=0$.

What emerges in our understanding of dimerization enhancement is a competition between the size of the $U=0$ gap and the valence bandwidth. $U$ separates charges and increases the negative spin correlation by mixing in excitations across the gap, enhancing the tendency to dimerize, while charge localization reduces the valence bandwidth, reducing dimerization by reducing the available electronic energy. As $\delta$ decreases from 0.10 to 0.05 in Fig. 5 the curve tails off less rapidly towards zero at high $U$ reflecting the diminishing importance of the bandwidth. At $\delta=0$, only the increasing Peierls instability is important. The peaks get smaller with $\delta$ as the gap a consequence of opening a gap and reducing the mixing of excitations across the gap. The peaks also shift to smaller $U$ with increasing $\delta$, since the valence bandwidth is smaller, even at $U=0$, so that it takes a smaller $U$ to flatten the valence band. We would expect the peak to disappear roughly when the gap equals the valence bandwidth at $\delta\sim\frac{1}{3}$, and at $U\sim 4\,|\,t\,|\,/3$. The peaks are shifted to higher $U$ for smaller size rings, since it takes larger $U$ to mix in configurations across the gap and the $4n+2$ rings converge more rapidly to the infinite system at higher $U$.

With this picture and our results in mind, we turn to previous work on dimerization enhancement. Dixit and Mazumdar[3] examined the effects of Coulomb interactions on the barrier between the two equivalent ground states in Fig. 1. Their approach is particularly useful for anticipating which symmetry breaking occurs in a given model and for rationalizing the enhanced dimerization for $U<4\,|\,t\,|$. They consider $\Delta\varepsilon=\varepsilon(\delta, U)-\varepsilon(0, U)$, the energy change due to $\delta$, and suppose $N=10$ rings to be sufficiently converged. As shown in Fig. 5, however, the $\varepsilon'$ curves have not converged by $N=10$ for the relevant range, $0.05<\delta<0.10$. The shift of the maximum enhancement to smaller $U$ at larger $\delta$ also requires going beyond their analysis.

With fairly good constraints on the curve for the infinite system in the region of $\delta$ relevant to PA, we next compare our results with the variational calculation of Baeriswyl and Maki[6] based on the Gutzwiller ansatz. Their results are exact at $U=0$ and breakdown for $U>4\,|\,t\,|$. The solid lines in Fig. 8 reproduce the data from Fig. 1 of their paper. Their $\delta_0$ and $U/t_0$ are the same as our $\delta$ and $U/t$ and $\lambda$ is defined below (6). We can translate estimates of the infinite curves from our results into their notation by, for example, picking $\lambda$ and finding $U$ or $\delta$ in Fig. 3 or 5 where the corresponding $\varepsilon'/\delta$ crosses the infinite curve. We find the dashed curves in Fig. 8 sketched through our estimated points for $\lambda=0.1$, 0.2, and 0.29. The horizontal error bars indicate the $U/|\,t\,|$ values consistent with $\delta=0.05$ or 0.10 in Fig. 5. The Gutzwiller ansatz is satisfactory to $U=|\,t\,|$ and predicts the shift of the maximum with increasing $\lambda$. The dimerization enhancement is exaggerated well before the obvious breakdown above $U=4\,|\,t\,|$.

In another study of dimerization enhancement, Hayden and Mele present data for a 16-site chain in Fig. 3 of Ref. 5. Their $\delta$ is half of ours and $\lambda$ is twice Baeriswyl and Maki's[6]. If we place their data in the context of Fig. 5 we can understand their unexpectedly small dimerization enhancement in the physical regime. We can imagine that a 16-site chain in Fig. 5 would be fairly flat at small $U$, show a slight enhancement, and then decrease. Similar behavior is expected on plotting $\delta(U/t)$ rather than $\varepsilon'(\delta, U)/\delta$.

We can place the intuitive picture of dimerization enhancement in the more general context of the effect of $U$ and $\delta$ on the electronic orbitals. At $U=0$, the electrons doubly occupy valence-band orbitals, while at large

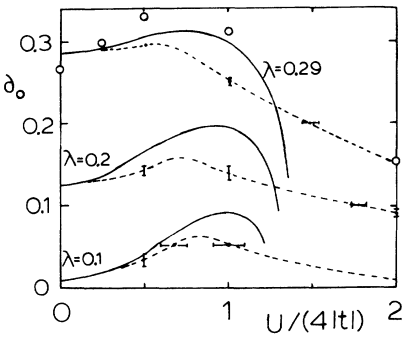


FIG. 8. Equilibrium dimerization $\delta_0$ vs $U/r\,|\,t\,|$ for $\lambda=0.1$, 0.2, and 0.29 [$\lambda=2\alpha^2/(\pi\,|\,t\,|\,K)$] from Baeriswyl and Maki's variational calculation (Ref. 6, solid curves), Hirsch's Monte Carlo calculation (open circles, Ref. 4), and our estimates (dashed lines, error bars).

$U$, electrons are localized on individual sites. To interpolate between the two limits, we start with the bands at $U=0$:

$$\varepsilon_k(\delta,0)/2\,|\,t\,|=\pm(\cos^2k+\delta^2\sin^2k)^{1/2}\ . \tag{10}$$

The dispersion is almost flat for $k$ within $\delta$ of $k_F=\pm\pi/2$. The flat regions increase with $\delta$ and allow construction of partially localized states with extension of order $\delta^{-1}$ at little cost in energy. $U$ presumably changes the partially localized to truly localized states, in the sense that they no longer extend to $x=\pm\infty$. Furthermore, $U$ mixes in singly occupied configurations involving localized states above the gap. Spins of electrons in the singly-occupied configurations above and below the gap are correlated as they are between neighboring sites. The connection between correlation of orbitals and sites is that linear combinations of localized states above and below the gap tend to produce interleaving orbitals sitting on alternate sites, since at $U=0$ such orbitals are related by a minus sign on alternate sites. Hopping between neighboring sites is converted to hopping between interleaving orbitals. As $U$ increases, more doubly occupied band states are converted to increasingly localized states with more singly occupied configurations and increasing total spin correlation. Increasing dimerization makes it less expensive to localize but more expensive to mix in excitations across the gap. At small $\delta$ (and moderate $U$) the gains outweight the additional costs and dimerization increases. At large $\delta$ the reverse is true, and at large $U$ states are already localized, so there is little gained by dimerizing.

## III. PPP MODEL AND MICROSCOPIC PARAMETERS

Hubbard models describe the evolution of band states to localized moments with increasing $U$. The motivation is conceptual and mathematical rather than physical realism for a particular system. The PPP model[10] for conjugated molecules, by contrast, attempts a unified and practical description for any $\pi$ system with specified $\sigma$-electron skeleton. The ZDO approximation[10] provides a consistent and convenient elimination of three-and four-center integrals, but its absolute accuracy remains open and any improvements may be illusory in view of the assumed $\sigma$-$\pi$ separation. The PPP model has long been the choice for molecular systems at the $\pi$-electron level. Its extension to conjugated polymers[1] is consequently natural.

The on-site $e$-$e$ term in (3) is augmented by Coulomb interactions in the ZDO approximation

$$H'=\frac{1}{2}{\sum_{pp'}}'\,V_{pp'}(1-n_p)(1-n_{p'})\ . \tag{11}$$

An empty or doubly-filled $2p_z$ orbital for carbons corresponds to a $C^+$ or $C^-$ site, respectively. The potential $V(R_{pp'})$ is interpolated from $U=V(0)=11.26$ eV, as suggested by the ionization potential and electron affinity of carbon atoms, to $e^2/R_{pp'}$ for distant sites according to the Ohno formula[26]

$$V(R)=U(1+R^2U^2/e^4)^{-1/2}\ . \tag{12}$$

Adding (11) to (3) and using (12) for $V_{pp'}$ fixes the PPP model. We retain linear $e$-ph coupling (4) and take an idealized chain with bond angles $\pi$. The $2\pi/3$ bond angles of PA result in slightly shorter second-neighbor separations. In contrast to extended Hubbard models,[27] where one or more $V_{pp'}$ are treated as independent parameters, the PPP model has a single nonadjustable $U$ in (12) that completely fixes both the magnitude and distance dependence of $V_{pp'}$.

The equilibrium dimerization in (2) now acquires a $\langle\partial V/\partial\delta\rangle$ contribution. We again change variables to the alternation $\delta=\alpha u/t$ and redefine $p(\delta,U)$ in (5) in terms of the PPP ground state. We regain the kinetic energy contribution $\Delta p(\delta,U)/\delta$ in (6), but the dimensionless ratio $|\,t\,|\,K/\alpha^2$ now also has a potential contribution

$$\frac{|\,t\,|\,K}{\alpha^2}=\frac{\Delta p(\delta,u)}{\delta}+\frac{1}{2N\,|\,t\,|}{\sum_{pp'}}'\frac{\partial V_{pp'}}{\partial\delta}\langle z_pz_{p'}\rangle\ . \tag{13}$$

The expectation values of the charge correlation functions $z_p=1-n_p$ simplify for a dimerized ground state. Since $R_{pp'}$ for even neighbors does not depend on $u$, $\partial V_{pp'}/\partial\delta$ vanishes for all even neighbors. In neutral (half-filled) systems, charge correlations decrease rapidly and $\langle z_p\rangle=0$ follows exactly from electron-hole symmetry. Thus the nearest-neighbor terms dominate in (13). Their coefficients are $V'(R_0\pm\delta t/\alpha)$. The $V'(R_0)$ term in the Taylor expansion leads to[12]

$$\frac{|\,t\,|\,K}{\alpha^2}=\frac{\Delta p(\delta,u)}{\delta}+\frac{V'(R_0)}{2\delta\,|\,t\,|}\langle z_2(z_1-z_3)\rangle\ , \tag{14}$$

where sites 1,2 and 2,3 have partial double and single bonds, respectively.

The numerical results below are based on all odd neighbors in (13). Their salient features are illustrated by the dominant nearest-neighbor terms in (14). We first note that $V'(R_0)$ and $\langle z_2(z_1-z_3)\rangle$ are both negative. Adjacent electron-hole pairs are more favored across partial double bonds than partial single bonds. Thus

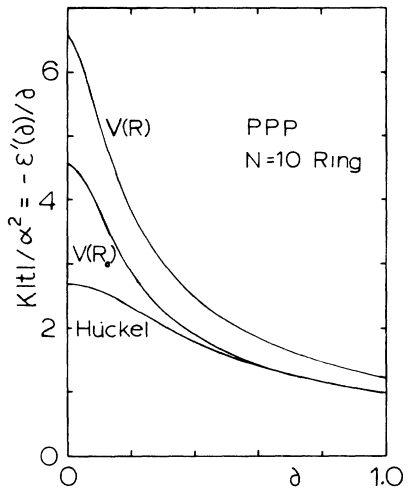


FIG. 9. Force constant $K$ for equilibrium dimerization $\delta$ in $N=10$ Hückel and PPP rings with potential $V(R)$ or potential $V(R_0)$ frozen at $\delta=0$.

$\langle z_2(z_1-z_3)\rangle$ vanishes at $\delta=0$ and is negative for $\delta>0$. The potential contribution always enhances dimerization. For weak $e$-$e$ correlations, when the ground state is close to the Hückel limit, we may explicitly evaluate (14). This amounts to first-order perturbation theory and leads to

$$\langle z_2(z_1-z_3)\rangle=-\Delta p(\delta,0)[p(\delta,0)+p(-\delta,0)]\ . \tag{15}$$

The logarithmic divergence of $\Delta p(\delta,0)/\delta$ in (7) also occurs in the potential contribution (15). An arbitrarily weak $e$-$e$ potential thus alters the Peierls instability by a factor of $1-\pi V'(R_0)/2\,|\,t\,|$ on taking $\delta\to 0$ in (15) and substituting into (14); any $V'(R_0)<0$ leads to enhancement. Such a term cannot occur in Hubbard models. The distance dependence of $V(R)$ has not been appreciated in extended Hubbard models, where in principle it could lead to a quite strong effect. Rather, the effects of *fixed* $V_1, V_2$, etc., are considered[3,8] on the dimerization, the nature of the ground state, or the effective $U$. Such contributions appear in the $\Delta p(\delta,U)/\delta$ term of (14), but not in $V'(R)$.

The linear term in the Taylor expansion of $V'(R_0\pm\delta t/\alpha)$, which was neglected in (14), remains finite for small $\delta$ even after dividing by $\delta$. The relevant charge correlations are now $\langle z_2(z_1+z_3)\rangle$, which are also well behaved as $\delta\to 0$. The $V'(R_0)$ term in (14) consequently dominates for small $\delta$.

The kinetic and potential energy contribution to $K\,|\,t\,|/\alpha^2=-\varepsilon'(\delta)/\delta$ are illustrated in Fig. 9 for $N=10$ site PPP rings. In each case, we adopt cyclic boundary conditions and measure $R$ in (12) along the circumference, always choosing the shorter length. Since changing $U$ in (12) changes the shape of the potential, we have focused on molecular, or standard, choices for $U$, $t$, and $\alpha$. The $U=0$ (Hückel) curve in Fig. 9 is the same as in Fig. 2 and shows the effects of a finite gap at $\delta=0$ in $4n+2$ rings. The intermediate curve is based on the PPP potential (12) frozen at $u=0$; in the frozen potential $V(R_0)$, all intersite separations are therefore multiples of $R_0$. The $V'$ terms in (13) are suppressed and we have correlation effects on $\Delta p(\delta,u)/\delta$ that generally parallel Hubbard model results. The correspondence can be made more precise, but not exact,[25] by defining an effective $U_e\simeq U-V(R_0)$ as done in extended Hubbard models. The possible distance dependence of $V(R)$ has not been considered, however. The final curve in Fig. 9 contains the full PPP Hamiltonian and shows the additional enhancement due to $V'$ in (13) or (14). This curve does not have the same dimer limit as the others because of the $R$ dependence of the potential.

In order to compare $N\to\infty$ results, we show $\delta=0.05$ and 0.10 data in Fig. 10 for $4n+2$ PPP rings and even chains. As discussed for Hubbard models, the rings converge from below, the chains from above. The extrapolated values are estimated as before. There is strong enhancement in PPP models, as already noted by Soos and Ramasesha.[9] The two- to threefold increase of $K\,|\,t\,|/\delta^2$, or of $-\varepsilon'(\delta)/\delta$, depends on both kinetic and potential-energy contributions. Though a value for $U_{\rm eff}$ in the Hubbard model is difficult to judge, the increased dimerization in comparison with *any* $U$ in Fig. 5 for $\delta=0.05$ and 0.10 Hubbard models shows the importance of $V'(R)$ terms. Most of the shift on including $V'(R_0)$ is common to all systems, reflecting its origin in the local nearest-neighbor part of $V(R)$. As for the $N=10$ case, the additional enhancement due to $V'(R_0)$ for $N\to\infty$ is comparable to enhancement for the fixed potential case.

Dimerization in PA clearly depends on the microscopic parameters $t$, $\alpha$, and $K$ in (1) plus any $e$-$e$ potential $V(R)$. The SSH choices for noninteracting electrons in Table I were chosen to fit the PA alternation $u_0\sim 0.04$ Å and optical gap, $E_g\sim 1.4$ eV. The Vanderbilt-Mele choices[28] retain the SSH model but also include observed C—C stretching frequencies related to $\varepsilon_T''(u_0)$ in Fig. 1. Three parameters $(\alpha,t,K)$ are optimized for three PA observations, $u_0$, $E_g=4\,|\,t\,|\,\delta$, and $\varepsilon_T''(u_0)$, none of which is very precise. Limited crystallinity leads to perhaps

TABLE I. Microscopic parameters for $\pi$-electron models: transfer integral $t$ at $R=R_0$, linear $e$-ph coupling constant $\alpha$, harmonic $\sigma$-electron force constant $K$, and $e$-$e$ potential $V(R)$ fixed at $U=V(0)$ in PPP models.

| | $t(R_0)$ (eV) | $\alpha$ (eV/Å) | $K$ (eV/Å$^2$) | $U=V(0)$ (eV) |
|---|---|---|---|---|
| SSH | 2.5 | 4.1 | 21.0 | |
| PPP and/or molecular | 2.40 | 3.21 | 24.6 | 11.26 |
| Vanderbilt-Mele | 3.0 | 8.0 | 68.6 | |

$\pm 0.01$ Å accuracy for $u_0$. The optical gap $E_g \sim 1.4$ eV was originally associated[13] with the band edge, but has recently been assigned[2] around 1.8 eV as other models account for the red edge down to $\sim 1.2$ eV. The curvature $\varepsilon_T''(u_0)$ is for a one-dimensional model rather than *trans*-$(CH)_x$ with coupled C-C and C-H vibrations. No other conjugated molecule or polymer is invoked, although the common features of all conjugated polymers is an important justification for detailed analyses of *trans*-PA. The PPP molecular choices in Table I have a completely different origin, as consensus values for small molecules that considerably predate current interest in conjugate polymers. Their application to PA involves no adjustable parameter.

Takahashi and Paldus[11] have examined $4n+2$ PPP rings from $n=1$ (benzene) to $n \sim 10-12$ for various self-consistent-field treatments. Their *e*-ph coupling $\alpha$ and force constant $K$ were fit to benzene data and represents a regular hexagon with a single minimum at $u=0$ in Fig. 1. Their values of $\alpha = 4.04$ eV/Å and $K = 27.5$ eV/Å$^2$ are close to the PPP choices in Table I. They also used a different interpolation, as $U(1+UR/e^2)^{-1}$ instead of (12), with $U = 10.84$ eV and an anharmonic lattice. Such corrections are well documented in polyenes.[29] The $4n+2$ rings developed a double minimum with increasing $n$ and both $u_0$ and $\varepsilon_T''(u_0)$ converged to values appropriate for *cis* and *trans* PA. Various self-consistent-field approximations for the ground-state energy $\varepsilon(\delta, U, N)$ lead to similar results that seem to be in good agreement with our exact $N=14$ results for a slightly different potential, geometry, and $\alpha$. They also recognized the importance of $V'(R_0)$ terms in increasing the effective value of $\alpha$. Thus molecular PPP parameters are consistent with the PA dimerization $u_0$ and C—C stretching frequencies $\varepsilon_T''(u_0)$. The proper inclusion of *e-e* correlations, by exact solution of ground and excited states of PPP models, overestimates[9] $E_g$ by $\sim 1.0$ eV. A red shift of $\sim 0.5$ eV due to the solid-state environment is not known precisely. While some small, $\sim 10\%$ reduction of $U$ in (12) would improve the PA fit, extensive reparametrization is not needed on going from conjugated molecules to conjugated polymers.

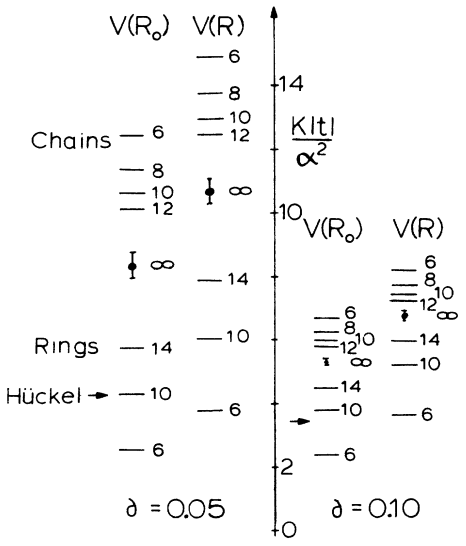


FIG. 10. Force constants $K$ for $\delta = 0.05$ and 0.10 PPP chains and rings with frozen potential $V(R_0)$ and full potential $V(R)$ in Eq. (12). The infinite Hückel value is marked by an arrow. The extrapolated $N \rightarrow \infty$ PPP values are indicated by closed circles and error bars.

## IV. DISCUSSION

We have focused on dimerization enhancement in Hubbard and PPP models. The lower bounds provided by $N=14$ rings unequivocally demonstrate enhanced dimerization in the alternation regime $\delta \sim 0.05-0.10$ relevant to PA, since the finite systems in Figs. 5 and 10 require a larger restoring force than the infinite Hückel chain. Our extrapolated results in Fig. 8 for Hubbard models show the enhancement to be smaller than previously thought. The contribution $V'(R_0)$ for the distance dependent PPP potential provides an enhancement comparable to the kinetic energy or bond order changes $\Delta p(\delta, u)/\delta$ in (6).

The mathematical analysis of other models, including more complicated choices for $V(R)$, for the electron-phonon coupling $\alpha$, for the $\sigma$-electron potential, or for dynamic *e*-ph coupling, is unlikely to be simpler than for Hubbard or PPP models. Thus, perturbative or variational arguments that are inadequate for the latter are hardly promising for more realistic models. Such models may nevertheless be required for conjugated polymers.

The SSH model and its continuum versions are effective Hamiltonians. As in Fermi liquid theory, the simplest parametrization is sought for the ground state and lowest excitations. The resulting parameters then include important many-body contributions. The dimerized PA ground state, $\varepsilon_T(u)$ in Fig. 1, is sufficiently simple that the principal features may also be obtained for PPP models. The Takahashi-Paldus analysis[11] for $u_0$ and $\varepsilon_T''(u_0)$, plus correlated state results for the optical gap and other excitations, indicate that molecular parameters are substantially preserved[1] in PA. Some reduction of correlations is possible although a distance dependent $V(R)$ must be kept. The reconciliation of molecular and polymeric parameters is important from a chemical point of view, where both are recognized to be conjugated systems. Such correspondences for excited states (solitons, polarons, or bipolarons) are far more difficult, however, and there models with noninteracting electrons offer more insight.

We consequently emphasize that any $\pi$-electron model based on (1) is sufficiently idealized to leave open questions about physical realism. More realistic treatments of $V(R)$, beyond the ZDO approximation in (11), have recently been proposed and discussed.[17] The bond-charge contribution, for example, reduces to the Coulomb exchange term for the two-site case retained by Kivelson, Su, Schrieffer, and Heeger.[17] Such contributions must be added to Hubbard models in order to describe ferromag-

netic interactions. The systematic inclusion of corrections terms to ZDO has been carried out by Wu, Sun, and Nasu[30] in terms of Jastrow-Feenberg variational theory. The range of the potential is important for dimerization enhancement or suppression. But previous experience with Hubbard models virtually requires more rigorous analysis of correlation contributions to dimerization. For the present, the PPP model is a convenient and consistent, if approximate, $\pi$-electron model with wide applicability.

## ACKNOWLEDGMENT

The financial support of this work under National Science Foundation Grant No. DMR-8403819 is gratefully acknowledged.

[1]Z. G. Soos and G. W. Hayden, in *Electroresponsive Molecular and Polymeric Systems*, edited by T. Skotheim (Dekker, New York, 1988), p.197.

[2]For reviews, see, *Handbook of Conducting Polymers*, edited by T. A. Skotheim (Dekker, New York, 1986), Vols. 1 and 2; Proceedings of the International Conference Science and Technology of Synthetic Metals, Kyoto, Japan, 1986, Synth. Met. **17-19** (1987). The author and subject indices are particularly useful.

[3]S. N. Dixit and S. Mazumdar Phys. Rev. B **29**, 1824 (1984), and references therein; S. Mazumdar and S. N. Dixit, Phys. Rev. Lett. **51**, 292 (1983).

[4]J. E. Hirsch, Phys. Rev. Lett. **51**, 296 (1983).

[5]G. W. Hayden and E. J. Mele, Phys. Rev. B **34**, 5484 (1986).

[6]D. Baeriswyl and K. Maki, Phys. Rev. B **31**, 6633 (1985), and references therein.

[7]S. Kivelson and D. Heim, Phys. Rev. B **26**, 4278 (1982).

[8]B. Horovitz and J. Sólyom, Phys. Rev. B **32**, 2681 (1985).

[9]Z. G. Soos and S. Ramasesha, Phys. Rev. B **29**, 5410 (1984).

[10]L. Salem, *The Molecular Orbital Theory of Conjugated Systems* (Benjamin, New York, 1966). A thorough and accessible discussion of work up to 1965.

[11]M. Takahashi and J. Paldus, Can. J. Phys. **62**, 1226 (1984), and references therein.

[12]Z. G. Soos and G. W. Hayden, Mol. Cryst. Liq. Cryst. **160**, 421 (1988).

[13]W. P. Su, J. R. Schrieffer, and A. J. Heeger, Phys. Rev. Lett. **44**, 1698 (1979); Phys. Rev. B **22**, 2099 (1980); W. P. Su, in *Handbook of Conducting Polymers*, Ref. 2, Vol. 2, p. 757.

[14]J. L. Black and V. J. Emery, Phys. Rev. B **23**, 429 (1981).

[15]E. H. Lieb and F. Y. Wu, Phys. Rev. Lett. **25**, 1445 (1968); A. A. Ovchinnikov, Zh. Eksp. Teor. Fiz. **57**, 2137 (1969) [Sov. Phys.—JETP **30**, 1160 (1970)].

[16]J. A. Pople, J. Chem. Phys. **37**, 3009 (1962); K. Ruedenberg, *ibid.* **34**, 1861 (1961).

[17]S. Kivelson, W. P. Su, J. R. Schrieffer, and A. J. Heeger, Phys. Rev. Lett. **58**, 1899 (1987); D. Baeriswyl, P. Horsch, and K. Maki, *ibid.* **60**, 70 (1988); J. T. Gammel and D. K. Campbell, *ibid.* **60**, 71 (1988).

[18]H. J. Longuet-Higgins and L. Salem, Proc. R. Soc. London, Ser. A **251**, 172 (1959).

[19]C. A. Coulson, Proc. R. Soc. London, Ser. A **169**, 413 (1939).

[20]Z. G. Soos, S. Kuwajima, and J. E. Mihalick, Phys. Rev. B **32**, 3124 (1985).

[21]K. Hashimoto, Int. J. Quantum Chem. **28**, 581 (1985).

[22]M. Hulthén, Ark. Mat. Astron. Fys. **26A**, 1 (1939).

[23]M. C. Cross and D. S. Fisher, Phys. Rev. B **19**, 402 (1979).

[24]For a review, see, J. W. Bray, L. V. Interrante, I. S. Jacobs, and J. C. Bonner, *Extended Linear Chain Compounds*, edited by J. S. Miller (Plenum, New York, 1983), Vol. 3, p. 353.

[25]S. Ramasesha and Z. G. Soos, Phys. Rev. B **32**, 5368 (1985).

[26]K. Ohno, Theor. Chim. Acta **2**, 219 (1964).

[27]G. Beni and P. Pincus, Phys. Rev. B **9**, 2963 (1974); S. Mazumdar and D. K. Campbell, Phys. Rev. Lett. **55**, 2067 (1985).

[28]D. Vanderbilt and E. J. Mele, Phys. Rev. B **22**, 3939 (1980).

[29]B. S. Hudson, B. E. Kohler, and K. Schulten, in *Excited States*, edited by E. Lim (Academic, New York, 1982), Vol. 6, p. 1.

[30]C. Wu, X. Sun, and K. Nasu, Phys. Rev. Lett. **59**, 831 (1987).